KSME Journal, Vol. 7, No. 3, pp. 185~193, 1993

The Structure of Turbulence in Pulsatile Pipe Flows

Manabu Iguchi*, Gil-moon Park and Young-ha Koh****

(*Received May 25, 1992*)

This paper describes the fundamental feature of pulsatile transitional and fully turbulent pipe flows. First, the effect of pulsation on the behavior of turbulent slugs in the developing region of circular pipe is clarified. Second, the distributions of turbulence intensity and Reynolds shear stress in fully turbulent pulsatile pipe flow are compared with their respective distributions in fully turbulent steady pipe flow. Generation region of turbulence and radial propagation time of the turbulence are determined from these distributions. Finally the turbulence structure in pulsatile pipe flows with and without relaminarization, i. e., reverse transition, is made clear by means of the conditional sampling method based on the four quadrant classification.

Key Words: Unsteady Flow, Pulsatile Pipe Flow, Turbulent Slug, Turbulence Structure, Conditional Sampling, Relaminarization

Nomenclature

A : Cross-sectional area of pipe
A_1 : Velocity amplitude ratio
D : Pipe diameter$=2R$
f : Pulsation frequency
N : Frequency
R : Pipe radius
Re_{ta} : Time-averaged Reynolds number$=\bar{u}_{m,ta} D/\nu$
t : Time
Δt : Time delay$\{=(\angle \bar{u}_{m,os,1} - \angle u'_{rms,os,1})/\omega\}$
u_m : Cross-sectional mean velocity
u'_{rms}, v'_{rms}, w'_{rms} : Root mean square values of axial, radial, and tangential turbulence components
$u_{*,ta}$: Time-averaged friction velocity
$\overline{u'v'}$: Reynolds shear stress divided by fluid density
x, r, θ : Axial, radial, tangential coordinates
y : Distance from wall
y^+ : $y\ \bar{u}_{*,ta}/\nu$
ν : Kinematic viscosity
ω : Angular frequency$=2\pi f$
ω^+ : Dimensionless frequency$=R^2\omega/\nu$

Subscripts and Others

c : Central value
g : Turbulence generation
os : Oscillating component
ta : Time-averaged value
$|\ |$, $\angle$: Amplitude and phase angle
$\bar{}$: Ensemble averaged value

* Department of Materials Science and Processing, Faculty of Engineering, Osaka University, 2-1 Yamada-oka, Suita, Osaka, 565, Japan
** Department of Mechanical Engineering, Chosun University, Kwangju 501-759, Korea

1. Introduction

Many investigations on pulsatile pipe flows have been made by Oka(1984), Tellonis(1981) and Ohmi et al.(1981) since the pioneering work of Sexl(1930). A conditional sampling technique was used to detect the difference of turbulence structure between pulsatile and steady turbulent pipe flows. The following facts were revealed. Turbulence was generated near the wall by the same ordered motions as those in a steady turbulent pipe flow and it propagated monotonically from the vicinity of the wall in the radial direction while decaying. The decay rate was not affected by pulsation. However, since the propa-

gation time to the pipe axis could not be ignored compared with the pulsation period, the instantaneous profiles of turbulence intensity and Reynolds shear stress differed significantly from their respective profiles in steady pipe flows. Most problems of laminar pipe flow have been solved analytically or numerically, and also the characteristics of mean flow of fully turbulent pipe flow is well understood. However, compared with pulsatile boundary layers on a flat plate by Hayakawa and Kobashi(1979) and Ovremski and Morkovin(1969), the detailed mechanism of transition to turbulence and the structure of turbulence in pulsatile pipe flows remain unknown, even in the case of well-used circular pipes.

2. Experimental Apparatus and Procedure

A schematic diagram of the experimental apparatus is shown in Fig. 1. Air was used as the working fluid. Steady flows and the time-averaged component of pulsatile flows were generated by means of a blower, and the oscillatory component of pulsatile flow were generated by means of a Scotch-yoke mechanism. The test pipe is a rigid and smooth brass pipe of 49.9 mm in diameter, 5 m in length and 5 mm in wall thickness. Three velocity components were measured at $x/D=99$ by making use of an I probe and two kinds of X probe, where x is the distance from the inlet and D is the pipe diameter. The ensemble-averaged value $\bar{u}$ and fluctuating component u' of the axial velocity, the fluctuating radial velocity v' and the fluctuating tangential velocity component w' were determined at 36 phase angles at equal intervals by using the data of cross-sectional mean velocity $\bar{u}_m$, root mean square values of the fluctuating component u'_{rms}, v'_{rms}, w'_{rms} and Reynolds shear stress $\overline{u'v'}$ were approximated by Fourier series having components up to the sixth harmonic. For example, $\bar{u}$ was represented by

$$\bar{u}=\bar{u}_{ta}+\sum_{n=1}^{6}|\bar{u}_{os,n}|\cos(n\omega t+\angle\bar{u}_{os,n}),$$

where the subscripts ta and os denote the time-averaged value over one pulsation period, and the oscillatory component, respectively, ω is the angular frequency and t is time. Meanwhile, velocity data were collected over 600 pulsation periods for the conditional sampling of u' and v'.

Experiments were made under $f=2.08$ Hz, $\omega'=23.5$, $Re_{ta}=3.86\times10^4$ and $A_1=0.925$, where $\omega'=R^2\omega/\nu$ is the dimensionless frequency, Re_{ta} is the time-averaged Reynolds number, and $A_1=|\bar{u}_{m,os,1}|/\bar{u}_{m,ta}$ is the velocity amplitude ratio. In defining ω', R is the pipe radius, ν the kinematic viscosity and the subscript 1 denotes the fundamental wave of the Fourier series.

3. Experimental Results and Discussion

3.1 Turbulence structure in fully turbulent pulsatile pipe flow

3.1.1 Turbulence intensity and Reynolds shear stress

Figure 2 shows the cross-sectional mean veloc-

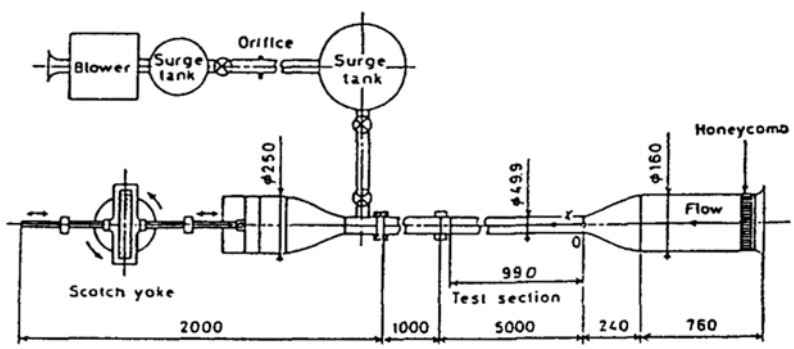

Fig. 1 Experimental apparatus

ity $\bar{u}_m$ changing almost sinusoidally. Three velocity components were obtained at 36 phase angles. Radial velocity distribution at every phase follows the universal logarithmic law as shown in Fig. 3. Figures 4 through 6 show the root mean square values of three turbulence components and Reynolds shear stress measured at representative four radial positions together with $\bar{u}_m$. Four kinds of lines denote quasi-steady values of u'_{rms}, v'_{rms}, w'_{rms} and $\overline{u'v'}$. Here the quasi-steady pipe flow is defined as the pulsatile pipe flow with infinitely long pulsation period, being determined on the basis of steady flow data. That is, the

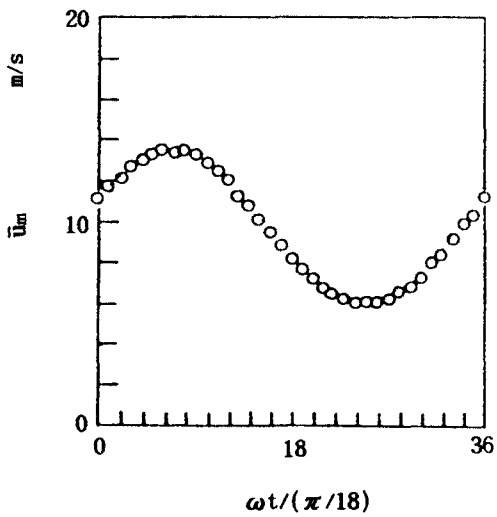

Fig. 2 Cross-sectional mean velocity in fully turbulent pipe flow

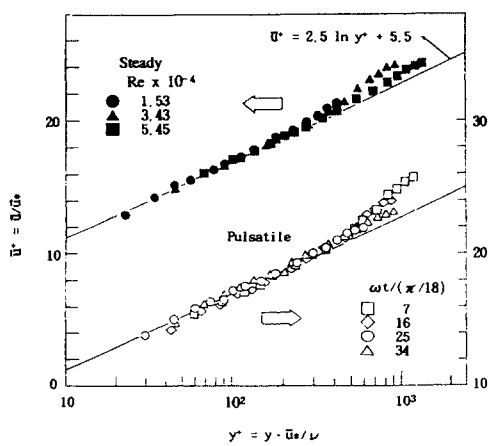

Fig. 3 Velocity profiles in the pipe cross-section

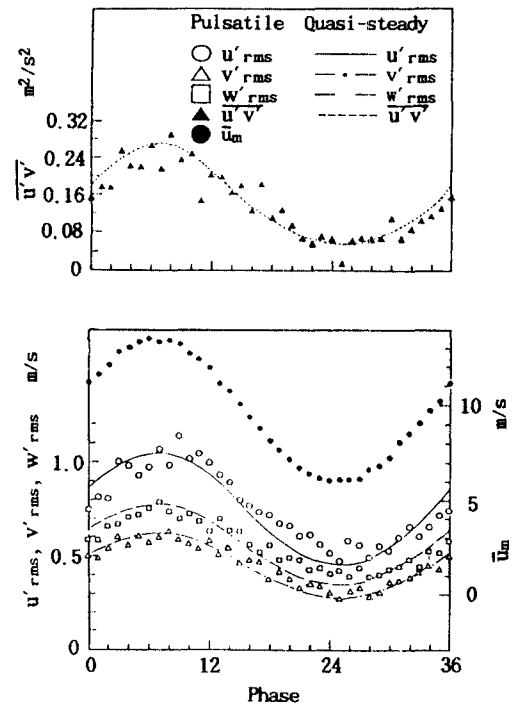

Fig. 4 Variation in three turbulence components and Reynolds shear stress at $r/R=0.9$

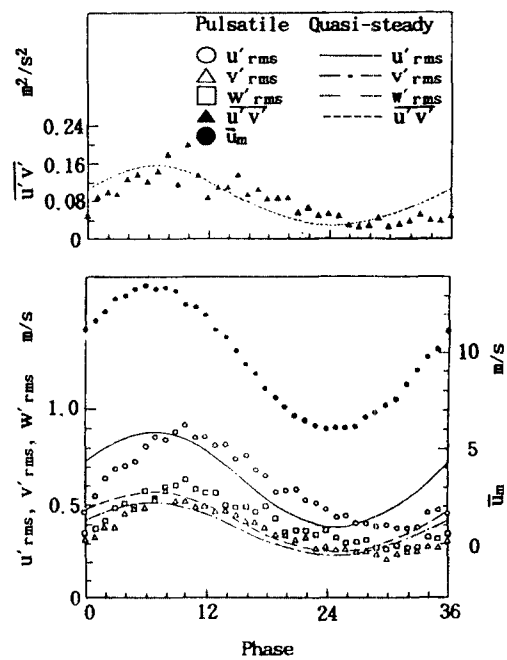

Fig. 5 Variation in three turbulence components and Reynolds shear stress at $r/R=0.5$

quasi-steady values of u'_{rms}, v'_{rms}, w'_{rms} and $\overline{u'v'}$ change in phase with the cross-sectional mean velocity $\bar{u}_m$. The measured values of these four quantities in pulsatile pipe flow follow their respective quasi-steady values near the pipe wall. But with increasing the distance from the pipe wall, they lag behind the quasi-steady variations.

Figures 7 and 8 show the time-averaged values and the amplitudes of the fundamental wave of u'_{rms}, v'_{rms}, w'_{rms}, respectively. The amplitude of each *rms* value almost equals to that of quasi-steady flow. The same tendency was observed for the Reynolds shear stress distribution. The phase difference is same for every turbulence component as can be seen in Fig. 9, but as a matter of course, no phase difference exists between *rms* values of quasi-steady flow and $\bar{u}_m$.

Owing to the phase differences shown in Fig. 9,

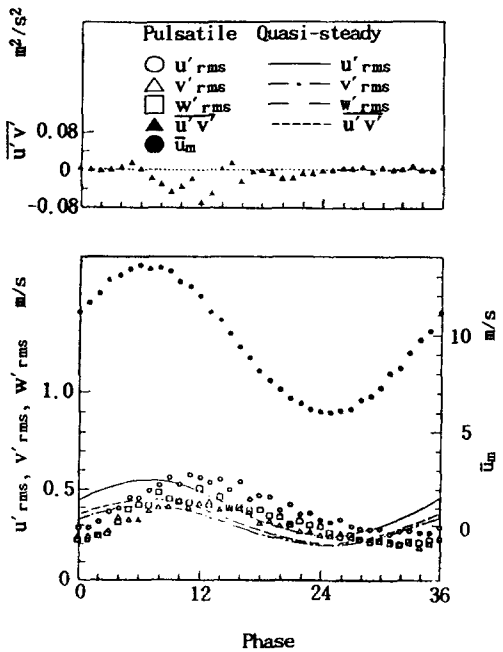

Fig. 6 Variation in three turbulence components and Reynolds shear stress at $r/R=0.0$

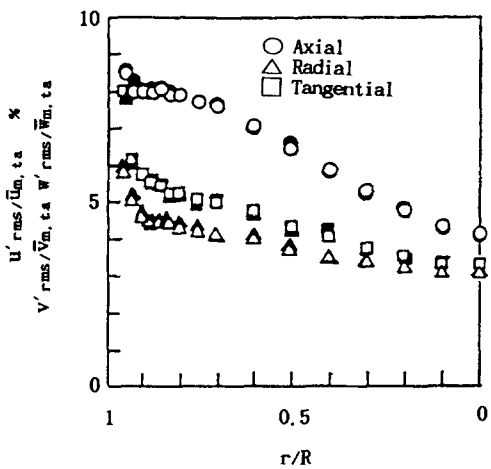

Fig. 7 Comparison of the time-averaged values of three turbulence components with those of quasi-steady flow (Solid symbols denote quasi-steady values)

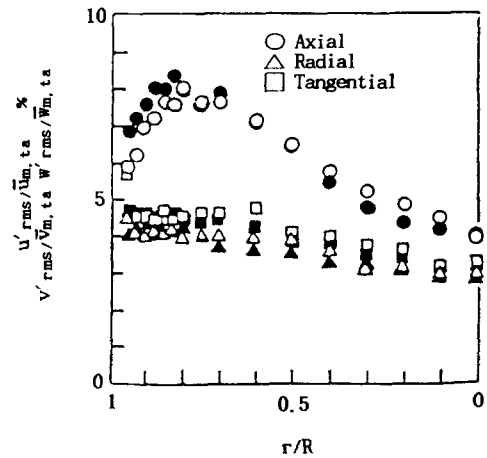

Fig. 8 Comparison of the fundamental amplitude of three turbulence components with those of quasi-steady flow (Solid symbols denote quasi-steady values)

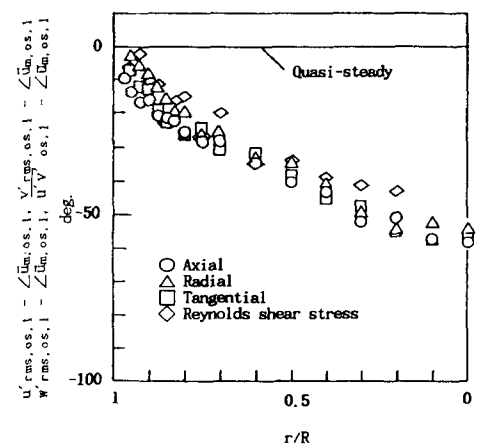

Fig. 9 Phase difference of three turbulence components and Reynolds shear stress

the instantaneous radial profiles of the *rms* values of turbulence components and Reynolds shear stress differ appreciably from their respective quasi-steady profiles.

3.1.2 Conditional sampling

Turbulent motions are classified into four distinct categories as shown in Fig. 10 : sweep, outward interaction, ejection and wallward interaction by Brodkey et al.(1974) and Hishida and Nagano(1981). Concerning steady pipe flows and boundary layers on a flat plate, it is said that turbulence is mainly produced by sweep and ejection. The aim of the present section is to reveal the difference between turbulent motions in steady flow and those in pulsatile pipe flow.

3.1.3 Structure of turbulence

Figures 11 to 14 show the frequency of occurrence of each motion, the contributions of each motion to the Reynolds shear stress, axial turbulence energy and radial turbulence energy. Solid lines in the figures represent steady flow data. The following conclusions can be derived from these experimental results and the phase difference data shown in Fig. 9.

Turbulence is generated near the wall by the same ordered motions as those in steady turbulent pipe flow. Iguchi(1988) proposed that the turbulence propagates monotonically from the vicinity of the wall in the radial direction while decaying. The decay rate is not affected by pulsation. Since the propagation time to the pipe axis can not be ignored compared with the pulsation period, the instantaneous profiles of turbulence intensity and Reynolds shear stress differ significantly from their respective profiles in steady pipe flows.

3.1.4 Radial propagation of turbulence

As shown above, the contributions of four turbulent motions to the axial and radial turbulence energies and Reynolds shear stress do not differ from steady flow. Therefore, the turbulence

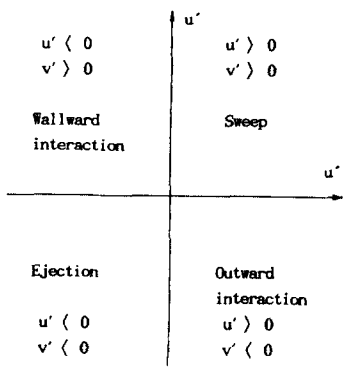

Fig. 10 Classification of turbulence motions in the u', v' plane

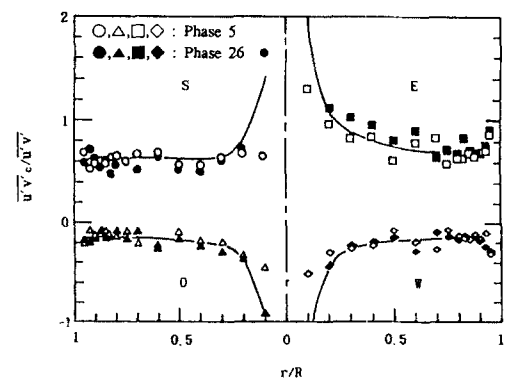

Fig. 12 Contribution to Reynolds shear stress

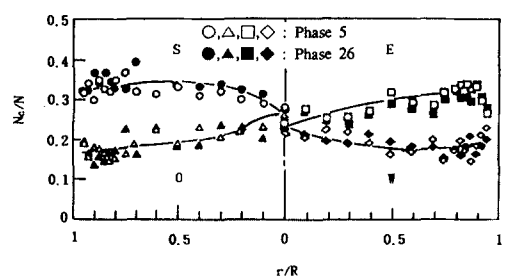

Fig. 11 Relative frequency (Capital letters S, O, E, W denote sweep, outward interaction, ejection, wallward interaction, respectively)

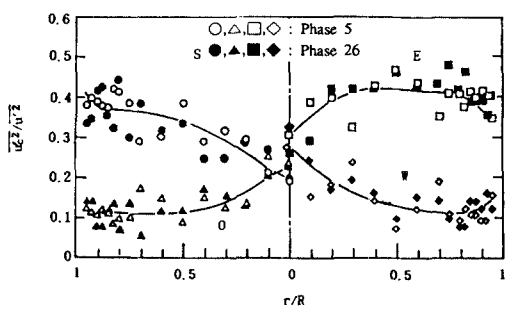

Fig. 13 Contribution to axial turbulence kinetic energy

structure of pulsatile turbulent pipe flows mentioned here becomes completely clear provided that the radial propagation time of turbulence is known.

Here, attention was paid mainly to low Reynolds number range by Iguchi and Miura(1989), because the radial propagation of turbulence was easy to observe under this condition.

The measured values of u'_{rms} were approximated by the following finite Fourier series.

$$u'_{rms}=u'_{rms,\,ta}+\sum_{n=1}^{6}|u'_{rms,\,os,\,n}|\cos(n\omega t+\Delta u'_{rms,\,os,\,n})$$

Figure 9 demonstrates that a time delay exists $\bar{u}_m$ and u'_{rms}. This time delay is denoted by Δt as shown schematically in Fig. 15. It is well known for steady flow that turbulence generation occurs mainly in a very narrow region near the wall called buffer layer or turbulence generation region by Corino and Brodkey(1969). However, it is assumed here, for simplicity, that turbulence is initiated at a position where a minimum Δt value appears. This position is termed the turbulence generation position and is designated by y_g, and the corresponding time delay is represented by Δt_g, where y is the distance from the wall, and the subscript g is used to denote the turbulence generation. The radial propagation of turbulence between y_g and any radial position is given by $\Delta t-\Delta t_g$.

Figure 16 shows the measured values of y_g^+, $\Delta t-\Delta t_g$ and Δt_g against the time-averaged Reynolds number Re_{ta}. Turbulence is mainly generated around $y^+=20$ and propagates toward the wall as well as the pipe center, where $y^+=20$ and propagates toward the wall as well as the pipe center, where $y^+=y\bar{u}_{*,ta}/\nu$, $\bar{u}_{*,ta}$ is the time-averaged friction velocity, and ν the kinematic

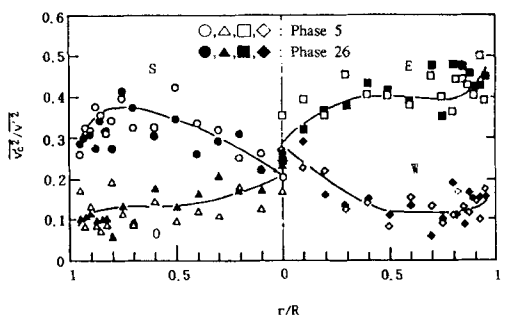

Fig. 14 Contribution to radial turbulence kinetic energy

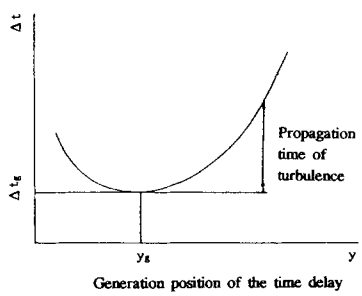

Fig. 15 Schematic representation of the time delay

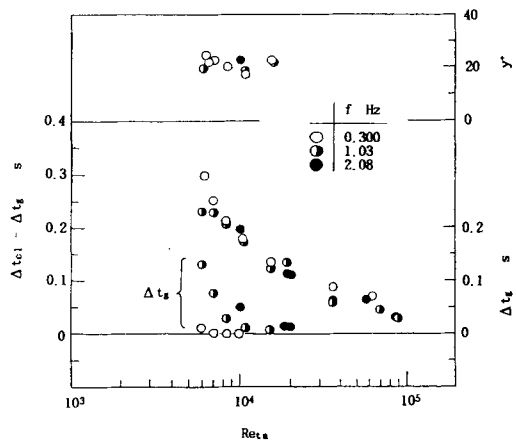

Fig. 16 Measured values of $\Delta t_{cl}-\Delta t_g$, t_g and y_g

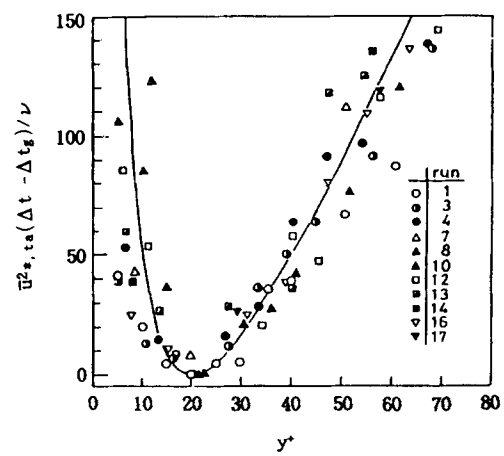

Fig. 17 Correlation to the propagation time of turbulence near the wall ——— : $\bar{u}^2_{*,ta}(\Delta t-\Delta t_g)/\nu=5(y^+-20)^2/y^+$

viscosity.

The propagation time near the generation region scales well with inner variables, $\bar{u}_{*,ta}$ and ν (Fig. 17), whereas in the central part of the pipe it scales with $\bar{u}_{*,ta}$ and pipe radius R (Fig. 18).

3.2 Thrbulence structure in pulsatile pipe flow accompanied by relaminarization

The cross-sectional mean velocity changes sinusoidally as seen from Fig. 19. The profiles of Reynolds shear stress divided by fluid density, $\overline{u'v'}$, are shown for four typical radial positions in Fig. 20. At every radial position $\overline{u'v'}$ is almost zero between phase 8 to phase 17, implying the cessation of turbulence production. An abrupt increase in $\overline{u'v'}$ can then be first seen at $r/R=0.9$. The phase where such an increase occurs is delayed as the radial distance from the wall increases. This fact indicates that turbulence generated near the wall propagates toward the pipe center. The measured values of turbulence shown in Figs. 21 to 23 decrease monotonically after phase 8. Such changes, which correspond to the

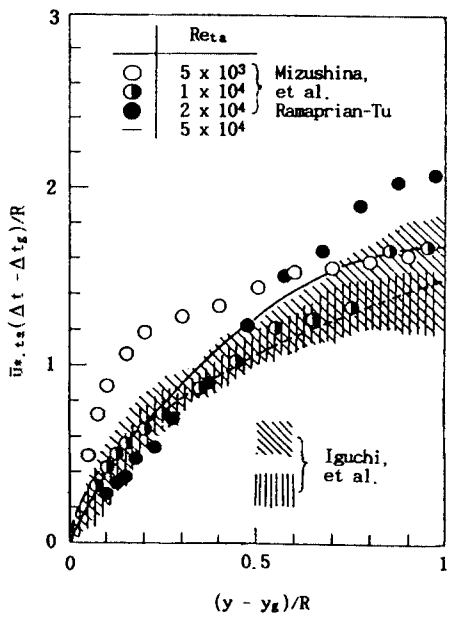

Fig. 18 Correlation of the propagation time of turbulence near the center-line, ----- : $\bar{u}_{*,ta}(\Delta t - \Delta t_g)/R = 1.5[(y-y_g)/R]^{1/2}$

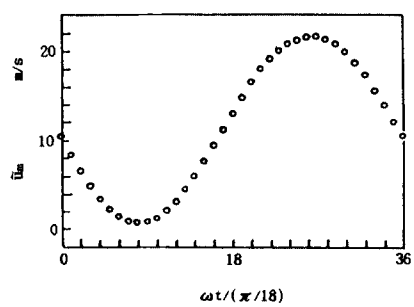

Fig. 19 Variation in cross-sectional mean velocity

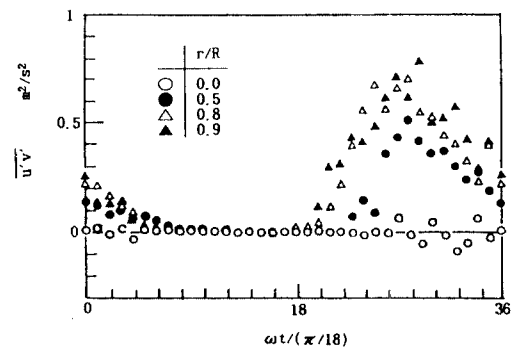

Fig. 20 Variation in Reynolds shear stress

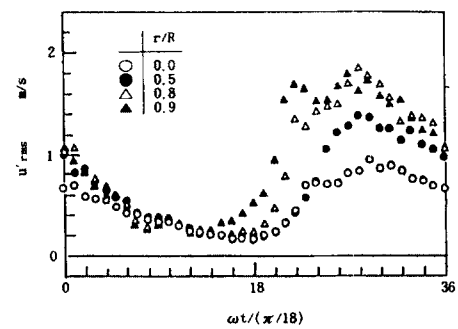

Fig. 21 Variation in axial turbulence intensity

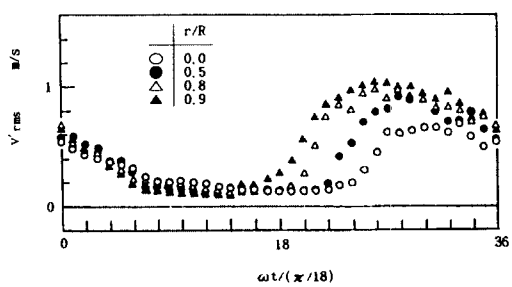

Fig. 22 Variation in radial turbulence intensity

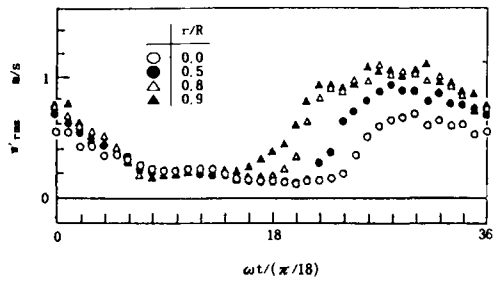

Fig. 23 Variation in tangential turbulence intensity

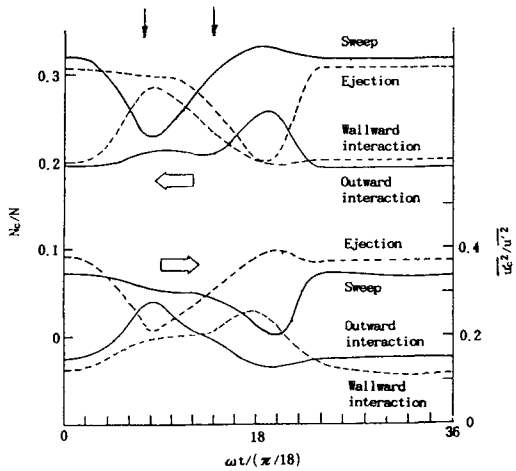

Fig. 24 Relative frequency of each motion and the contribution of each motion to axial turbulence kinetic energy

change in Reynolds shear stress in Fig. 20, also support the cessation of turbulence production there.

Experimental results based on the conditional sampling method are shown in Fig. 24. The contributions of sweep and outward interation to the Reynolds shear stress and the turbulence energy are dominant in the earliest stage of the accelerating period where the ordered motions called bursting cease due to a combined effect of viscosity and acceleration. The ejection and the wallward ineraction play an important role when the production of turbulence occurs in the last stage of the accelerating period. Turbulence generated near the wall has propagated to the pipe axis around this phase. The measured values of relative frequency and of contributions to turbulence kinematic energy and Reynolds shear stress are in agreement with profiles of steady flow. This agreement can be observed until about phase 5. Therefore, the turbulence structure during the period when turbulence covered the whole cross section is the same as that of steady flow. The same structure was seen in fully turbulent pulsatile pipe flows with $f=2.08$ Hz.

4. Conclusions

The results obtained from these experimental studies are summarized as follows :

(1) Radial velocity distribution at every phase follows the universal logarithmic law.

(2) The measured values of u'_{rms}, v'_{rms}, w'_{rms} and $\overline{u'v'}$ in pulsatile pipe flow follow their respective quasi-steady values near the pipe wall. But with increasing the distance from the wall, they lag behind the quasi-steady variations.

(3) From the late stage of the accelerating period to the late stage of the decelerating turbulence is produced by the same mechanism as steady flow.

(4) Sweep and outward interaction dominate the contributions to turbulence kinematic energy and Reynolds shear stress, though their relative frequencies are small.

(5) The relative frequency of outward interaction remains about 0.25. The relative frequency of sweep increases appreciably and those of ejection and wallward interaction decreases from 0.25. Ejection and wallward interaction dominate the contributions to turbulence kinetic energy, though their relative frequencies are very small.

(6) Turbulence is mainly generated around $y^+=20$ and propagates toward the wall as well as the pipe center. And turbulence structure after turbulence has reached the pipe center.

The pulsation frequency of pulsatile pipe flows mentioned here is about one order of magnitude as small as the mean burst frequency. If the pulsation frequency is comparable to or greater than the mean burst frequency, the behavior of turbulent slug and turbulence structure might differ from the present results. Further work on these subjects is desirable.

References

Brodkey, R. S. et al., 1974, J. Fluid Mech., 63 -2, p. 209.

Corino, E. R. and Brodkey, R. S., 1969, J. Fluid Mech., 37-1, p. 1.

Hayakawa, M. and Kobashi, Y., 1979, Trans, Jpn. Soc. Mech. Eng. (in Japanese), 45-389, B, p. 46.

Hayakawa, M. and Kobashi, Y., 1979, "Trans. Jpn. Soc. Mech. Eng. (in Japanese), 46-411, B, p. 46.

Hayakawa, M. and Nagano, Y., 1981, "Trans. Jpn. Soc. Mech. Eng. (in Japanese), 47-413, B, p. 50.

Iguchi, M., 1988, JSME International Journal, Ser, II, 31-4(1988), P. 623.

Iguchi, M. and Miura, H., 1989, JSME International Journal, Ser. II, 32-2, p. 173.

Iguchi, M., Ohmi, M. and Takeuchi, H., 1987, Trans. Jpn. Soc. Mech. Eng. (in Japanese), 53 -487, B, p. 706.

Kobashi, Y. and Onji, A., 1964, Technical Report of National Aerospace Laboratory TR-65, p. 1.

Miller, J. A. and Fejer, A. A., 1964, J. Fluid Mech., 18-3, p. 438.

Nakagawa, K., Kobashi, Y. and Hayakawa, M., 1977, Trans. Jpn. Soc. Mech. Eng. (in Japanese), 43-367, p. 1005.

Nakagawa, K., Kobashi, Y. and Hayakawa, M., 1978, Trans. Jpn. Soc. Mech. Eng. (in Japanese), 44-388, B, P. 4206.

Obremski, H. J. and Fejer, A. A., 1967, J. Fluid Mech., 29-1, p. 93.

Obremski, H. J. and Morkovin, M. V., 1969, AIAA J., 7-7, p. 1298.

Ohmi, M. and Iguchi, M., 1981, Trans. Jpn. Soc. Mech. Eng. (in Japanese), 48-430, B, p. 981.

Oka, S., 1984, Biorheology, Syokabo Book Co., Tokyo.

Sexl, T., Z. 1930-5, Phys., 61-1/7, p. 349.

Tellonis, D. P., 1981, Unsteady Viscous Flows, Springer-Verlag, New York.